Measurement of the ^{157}Gd(n,γ) reaction with the DANCE γ calorimeter array

A. Chyzh, B. Baramsai, J. A. Becker, F. Bečvář, T. A. Bredeweg, A. Couture, D. Dashdorj, R. C. Haight, M. Jandel, J. Kroll, M. Krtička, G. E. Mitchell, J. M. O'Donnell, W. Parker, R. S. Rundberg, J. L. Ullmann, D. J. Vieira, C. L. Walker, J. B. Wilhelmy, J. M. Wouters, and C. Y. Wu

Phys. Rev. C **84**, 014306 — Published 8 July 2011

DOI: 10.1103/PhysRevC.84.014306

Measurement of the ^{157}Gd(n,γ) reaction with the DANCE array

A. Chyzh,[1,2] B. Baramsai,[1] J. A. Becker,[2] F. Bečvář,[3] T. A. Bredeweg,[4] A. Couture,[4] D. Dashdorj,[1,2] R. C. Haight,[4] M. Jandel,[4], J. Kroll,[3] M. Krtička,[3] G. E. Mitchell,[1] J. M. O'Donnell,[4] W. Parker,[2] R. S. Rundberg,[4] J. L. Ullmann,[4] D. J. Vieira,[4] C. L. Walker,[1] J. B. Wilhelmy,[4] J. M. Wouters,[4] C. Y. Wu.[2]

[1] *North Carolina State University, Raleigh, North Carolina 27695, USA and Triangle Universities Nuclear Laboratory, Durham, North Carolina 27708, USA*

[2] *Lawrence Livermore National Laboratory, Livermore, California 94551, USA*

[3] *Charles University in Prague, Faculty of Mathematics and Physics, V Holešovičkách 2, 180 00 Prague 8, Czech Republic and*

[4] *Los Alamos National Laboratory, Los Alamos, New Mexico 87545, USA*

The ^{157}Gd(n,γ) reaction was measured with the DANCE γ calorimeter (consisting of 160 BaF_2 scintillation detectors) at the Los Alamos Neutron Science Center. The multiplicity distributions of the γ decay were used to determine the resonance spins up to E_n = 300 eV. The γ-ray energy spectra for different multiplicities were measured for the *s*-wave resonances. The shapes of these spectra were compared with simulations based on the use of the DICEBOX statistical model code. Simulations showed that the scissors mode is required not only for the ground-state transitions but also for transitions between excited states.

PACS numbers: 28.20.Np, 27.60.+j, 25.40.Lw, 25.40.Ny, 24.60.Dr, 24.10.Pa

I. INTRODUCTION

In medium and heavy mass nuclei detailed spectroscopic information exists only for levels at low excitation energy near the ground state or for resonances above the neutron separation energy B_n. Due to the rapid increase of the level density with excitation energy, it is extremely difficult to resolve the populating or depopulating transitions in order to obtain reliable spectroscopic information in this intermediate energy region below B_n. The set of these levels is often called a *level quasicontinuum*. It is believed that γ decay of the nucleus in the quasicontinuum is described by the extreme statistical model in terms of the nuclear level density and a set of photon strength functions (PSFs) for different multipolarities. Probably the most direct way to examine these quantities is via study of the properties of γ-ray spectra originating from the radiative neutron capture reaction at isolated resonances.

The combination of the pulsed neutron beam at LANSCE (**L**os **A**lamos **N**eutron **S**cience **CE**nter) and the highly segmented, highly efficient γ calorimeter DANCE (**D**etector for **A**dvanced **N**eutron **C**apture **E**xperiments) provides an ideal opportunity to study the γ-ray cascades.

In the present paper we describe a measurement of the ^{157}Gd(n,γ)^{158}Gd reaction using the DANCE calorimeter. This experiment is part of a series of experiments that measure neutron capture in all of the stable gadolinium isotopes. A major goal is to use γ-ray spectra for various multiplicities to determine the appropriate photon strength functions with special interest in the behavior of the scissors mode. In turn this information should shed light on the relevant nuclear structure. In addition we wished to use the high segmentation of the DANCE array to determine the spins of the capturing resonance states from the measured multiplicity distribution of their γ decay.

In Sec. II the experimental technique to measure the γ spectra is described. The modeling of the statistical γ cascades is discussed in Sec. III. Determining the resonance spins is considered in Sec. IV. Information about the photon strength functions that can be obtained from the measured γ-ray spectra is presented in Sec. V and briefly compared with other available data in Sec. VI. A summary is given in Sec. VII.

II. EXPERIMENTAL SETUP AND MEASUREMENTS

A. Experimental setup

The experiment was performed at the neutron source LANSCE [1]. The 800-MeV H^- beam from the LANSCE linac is injected into the proton storage ring where it is immediately converted to H^+ by stripping through a thin foil. The proton bunches are stacked for the entire linac macropulse. This pulsed beam is then extracted with a repetition rate of 20 Hz and strikes a tungsten spallation target. The resulting fast neutrons are moderated and sent to flight path 14 at the Manuel Lujan Jr. Neutron Scattering Center. The DANCE detector array is installed at 20 m on this flight path.

The DANCE spectrometer [2, 3] is designed for studying neutron capture cross sections on small samples. DANCE consists of 160 BaF_2 scintillation crystals surrounding a sample and subtending a solid angle of $\simeq 4\pi$. A ^{6}LiH shell about 6-cm thick is placed between the sample and the BaF_2 crystals in order to reduce the scattered neutron flux striking the crystals. The remaining background due to scattered neutrons that penetrate the ^{6}LiH shell and interact with the BaF_2 crystals is subtracted in the off-line analysis. Besides the BaF_2 crystals, the

TABLE I: Isotopic composition of the Gd target used in the measurements.

Target	Isotope abundance (%)						
	^{152}Gd	^{154}Gd	^{155}Gd	^{156}Gd	^{157}Gd	^{158}Gd	^{160}Gd
^{157}Gd	<0.01	<0.01	0.08	0.09	99.7	0.12	<0.01

DANCE setup includes three additional detectors that are used to monitor the neutron flux, and one detector for monitoring the external background.

The target was gadolinium deposited via electroplating on a beryllium foil glued to an aluminum ring. The isotopic composition of the target is listed in Table I. The average thickness of the gadolinium, as determined by the α-backscattering technique, is approximately 0.8 mg/cm^2, but is highly nonuniform: the difference in thickness between the edges and the center of the target varies by as much as a factor of four.

B. Data processing

1. On-line data processing

The DANCE acquisition system [4] is based on waveform digitization of signals from all 160 detectors using four-channel Acqiris DC265 digitizers with a sampling rate of 500 MS/s (mega samples/second). The intensity of the signal from a specific crystal is collected in using a digitizer channel with suitably adjusted gains. The ratio of the fast and slow components of the signal is used for discrimination against the α-background from natural radioactivity of Ra in the BaF_2 crystals [3]. The digitizers are arranged in 14 compact PCI crates with six DC265 modules per crate. Thus one crate can handle 12 BaF_2 detectors with two channels per detector. Each crate contains an embedded computer running under the Linux operating system, and a front-end acquisition program using the framework known as Maximum Integrated Data Acquisition System (MIDAS) [5].

2. Off-line data processing

The energy calibration of the DANCE crystals was performed with a combination of γ-ray sources: 662 keV from ^{137}Cs, 898 keV from ^{98}Y, and 1275 keV from ^{22}Na and the intrinsic radioactivity of the detector material (^{226}Ra). The latter calibration was conducted on a run-by-run basis to provide the energy alignment of all crystals in the off-line analysis.

Typical spectra of sums of deposited γ-ray energies in crystals that fire are shown in Fig. 1. As only s-wave neutron capture plays a role at low neutron energies in this mass region, in this experiment we observe only resonances with $J^\pi = 1^-$ and 2^-. Each spectrum consists of (i) the "total" peak at the full energy available from

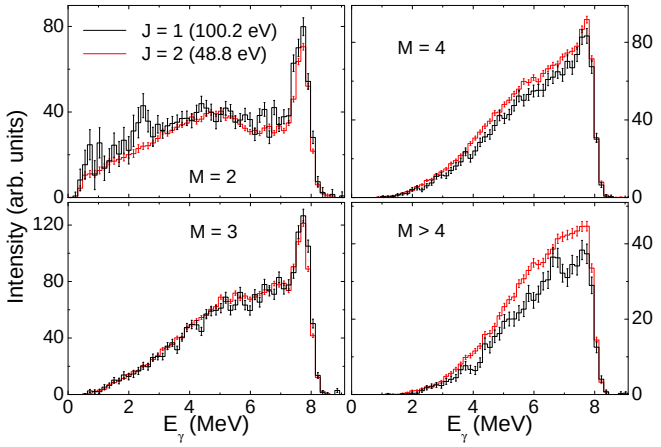

FIG. 1: (Color online) Examples of sum-energy spectra for resonances at energies of 100.2 and 48.8 eV with J^π assignments 1^- and 2^-, respectively. The cluster multiplicities of the γ cascades, M, are indicated. The spectra are normalized to the intensity in the $E_{\rm total}$ peak for multiplicities $M = 2-7$.

the neutron capture reaction

$$E_{\rm total} = B_n + E_n, \quad (1)$$

where $B_n = 7.937$ MeV and E_n is the energy of the incoming neutron in the center of mass, and (ii) a low energy tail that corresponds to cascades for which a part of the emitted energy escaped the detector array. The shape of the spectrum at low sum energies (below about 3 MeV), is strongly influenced by the background from natural β activity in the BaF_2 crystals, especially for low multiplicities.

Often an emitted capture γ ray does not deposit its full energy in one crystal. Thus the number of crystals that fire is usually higher than the true multiplicity of a capture event. Therefore all contiguous crystals that have fired during an event are combined and considered as the response of the detector array to one single γ-ray. The number of clusters observed in a capture event is called the "cluster" multiplicity. This multiplicity is much closer to the true multiplicity of the γ cascade than is the "crystal" multiplicity (the total number of crystals that fire). The capture events in the off-line analysis were sorted using gates on neutron energy and on the cluster multiplicity.

Only events within a certain range of detected sum energies E_Σ (around the $E_{\rm total}$ peak) were taken into account. Namely, for the spin assignments a sum-energy range $E_\Sigma = 5.0 - 8.1$ MeV, while for analysis related to the PSFs a narrower interval $E_\Sigma = 7.0 - 8.1$ MeV was chosen for construction of multistep cascade spectra. In the latter case the use of a wider interval improves statistics but leads to significant smearing of the structures seen in the spectra. Additional narrowing of the interval has no impact on the spectral shape.

There is a background contribution in the spectra that mainly originates from γ rays following the capture of

scattered neutrons in the barium detectors. The size of the background was estimated using the number of counts for E_Σ above the $E_{\rm total}$ region in the sum-energy spectra. The background contribution from other Gd isotopes is negligible due to the purity of the target. For the strong resonances used for determining the PSFs, the background contribution can be neglected.

III. SIMULATIONS OF THE γ-DECAY OF ^{158}GD

A. Simulations of Spectra

Under various assumptions about the level density and photon strength functions the γ cascades following resonant neutron capture were generated using the DICEBOX algorithm [6]. The response of the DANCE detector to each generated cascade was subsequently obtained from a simulation based on the use of a code based on the GEANT4 package. All materials in the detector system were included in the GEANT4 simulations [7]. The resulting quantities can be compared with their experimental counterparts. We used the simulations primarily to obtain information on the PSFs, but they were also used to test the possibility of resonance spin determination.

The DICEBOX algorithm generates a complete decay scheme of an artificial nucleus. Below some critical energy, $E_{\rm crit}$, all of the characteristics of the decay scheme, i.e., energies, spins and parities of levels, as well as their decay properties, are taken from existing experimental data. The choice of the critical energy should be made with care to guarantee that all of the information for energies below $E_{\rm crit}$ is complete. We took the required data from [8] and adopted $E_{\rm crit} = 2.1$ MeV. Above $E_{\rm crit}$ the level system of the nucleus and its complete decay scheme are generated using an *a priori* chosen level density function $\rho(E, J, \pi)$ and PSFs for multipolarities $E1$, $M1$, and $E2$. All higher multipolarities are neglected. Partial radiation widths $\Gamma_{a\gamma b}$ for a transition between an initial level a and a final level b are given by

$$\Gamma_{a\gamma b} = \sum_{XL} \frac{\xi^2_{XL} f^{(XL)} E_\gamma^{2L+1}}{\rho(E_a, J_a, \pi_a)}, \qquad (2)$$

where $f^{(XL)}$ stands for photon strength function for transitions of type X (electric or magnetic) and multipolarity L, and ξ_{XL} is a random number generated from a normal distribution with zero mean and unit variance. This random number ensures that the individual widths $\Gamma_{a\gamma b}$ fluctuate according to the Porter-Thomas distribution [9]. The sum in Eq. (2) is over all allowed types and multipolarities of transitions. Internal electron conversion, which is important in transitions between the lowest excited states in 158Gd, is correctly treated in the DICEBOX code [6].

Hereafter the simulated system of all levels and their decay scheme is called a *nuclear realization*. Due to the Porter-Thomas fluctuations there is an infinite number of nuclear realizations that differ from each other even for fixed models of PSFs and level density.

Various models of PSFs and level density can be tested with the DICEBOX code. The fluctuations involved in generating the γ decay allow us to determine all of the uncertainties that arise when simulations are performed with the same models. Cascades starting from resonances with a given spin and parity were simulated. Typically 20 nuclear realizations, each with 100,000 cascades, were simulated for initial s-wave resonances, i.e., those with spins $J^\pi = 1^-$ and 2^-.

Among the various kinds of information that can be obtained from the combined DICEBOX+GEANT4 simulations, of special interest are the average multiplicities, the multiplicity distributions, and the so-called multistep cascade (MSC) spectra, see Sec. V.

In our trial-and-error approach, by assuming various models for the PSFs and the level density we can assess the degree of agreement of the simulated observables with the experimental data and draw conclusions about which of these models is most likely to be valid.

B. Photon Strength Functions

1. Electric-dipole transitions

Decay of the neutron resonances is dominated by dipole transitions. It is well known that for γ-ray energies above neutron separation energies the electric-dipole ($E1$) transitions play a major role. The PSF at these energies in axially deformed nuclei seems to be consistent with the sum of two Lorentzian terms

$$f^{(E1)}_{\rm SLO}(E_\gamma) = \frac{1}{3(\pi\hbar c)^2} \sum_{i=1}^{2} \frac{\sigma_{G_i} E_\gamma \Gamma^2_{G_i}}{(E_\gamma^2 - E^2_{G_i})^2 + E_\gamma^2 \Gamma^2_{G_i}}. \qquad (3)$$

Here E_{G_i}, Γ_{G_i}, and σ_{G_i} are the parameters of the Giant Electric Dipole Resonance (GEDR) which is split into two components ($i = 1$ and 2) in well-deformed nuclei. The parameters $E_G = 12.23$ and 15.96 MeV, $\Gamma_G = 2.77$ and 5.28 MeV and $\sigma_G = 215$ and 233 mb were adopted – they come from a fit of photonuclear data on the ground state of the nearby nucleus ^{160}Gd [10]. This PSF shape combined with the Brink hypothesis [11] – which says that the PSF shapes are independent of excitation energy – is known as the Brink-Axel or Standard Lorentzian (SLO) model.

Since the shape of the $E1$ PSF below the neutron separation energy is not well known, additional models are employed. Usually one of two models is used. The first one was proposed by Kadmenskij, Markushev and Furman (KMF) [12] for spherical or weakly deformed nuclei, but is often also used for deformed nuclei

$$f^{(E1)}_{\rm KMF}(E_\gamma, T) = \frac{F_K}{3(\pi\hbar c)^2} \sum_{i=1}^{2} \frac{\sigma_{G_i} E_{G_i} \Gamma_{G_i} \Gamma(E_\gamma, T)}{(E_\gamma^2 - E^2_{G_i})^2}, \qquad (4)$$

where the factor $F_K = 0.7$ [12, 13] and the γ-ray- and temperature-dependent width $\Gamma(E_\gamma, T)$ is given by

$$\Gamma(E_\gamma, T) = \Gamma_{G_i} \frac{E_\gamma^2 + 4\pi^2 T^2}{E_{G_i}^2}, \quad (5)$$

with temperature $T = T(E) \equiv \sqrt{(E-\Delta)/a}$, E is the excitation energy of a final level, Δ the pairing energy, and a the shell-model level-density parameter. The values $\Delta = 1.77$ MeV and $a = 17.91$ MeV^{-1} were adopted from [14].

A second model was proposed for spherical nuclei by Chrien [15] in order to match the behavior of the SLO model at energies near the GEDR maximum and the KMF model at very low E_γ. This phenomenological model was later generalized for deformed nuclei by Kopecky *et al.* [16] by introducing an empirical enhancement factor k_0. This model is known as the EGLO (Enhanced Generalized Lorentzian) model. In this case the expression for the PSF is

$$f_{\rm EGLO}^{(E1)}(E_\gamma, T) = \sum_{i=1}^{2} \frac{\sigma_{G_i}\Gamma_{G_i}}{3(\pi\hbar c)^2} \left[\frac{4\pi^2 F_K \Gamma_{G_i} T^2}{E_{G_i}^5} + \frac{E_\gamma \Gamma(E_\gamma, T)}{(E_\gamma^2 - E_{G_i}^2)^2 + E_\gamma^2 \Gamma(E_\gamma, T)^2} \right]. \quad (6)$$

Here the γ-ray- and temperature-dependent width is given by

$$\Gamma(E_\gamma, T) = \left[k_0 + \frac{E_\gamma - E_{\gamma 0}}{E_G - E_{\gamma 0}}(1 - k_0) \right] \Gamma_{G_i} \frac{E_\gamma^2 + 4\pi^2 T^2}{E_{G_i}^2}. \quad (7)$$

The recommended value of $E_{\gamma 0}$ is 4.5 MeV [13, 16]; in Ref. [13] the systematics of the parameter k_0 was adjusted to reproduce the total radiation width of neutron resonances. As the total radiation width depends on the number of levels below neutron separation energy the suggested systematics of k_0 depends on the proposed level density model. We left the parameter k_0 free to vary in our simulations. The energy dependence of the EGLO model is very similar to the KMF model for $k_0 \approx 1.5$.

Many other models of $E1$ PSF can be found in the literature. RIPL-3 database [17], probably the most widely used database by experimentalists, suggests that the MLO family of models be used. As the description of these models is rather complicated, the reader is referred to their detailed description in Ref. [17].

As seen from Eqs. (4) and (6) the shapes of both the KMF and EGLO models depend on temperature (or excitation energy) of the decaying nucleus and violate the strict form of the Brink hypothesis. Similar temperature dependence of $E1$ PSF is also a feature of the MLO family of models. The energy dependence of the PSFs predicted by these models is shown in Fig. 2. To keep the figure reasonably clear we show only the shape of one of the MLO models (MLO2) here.

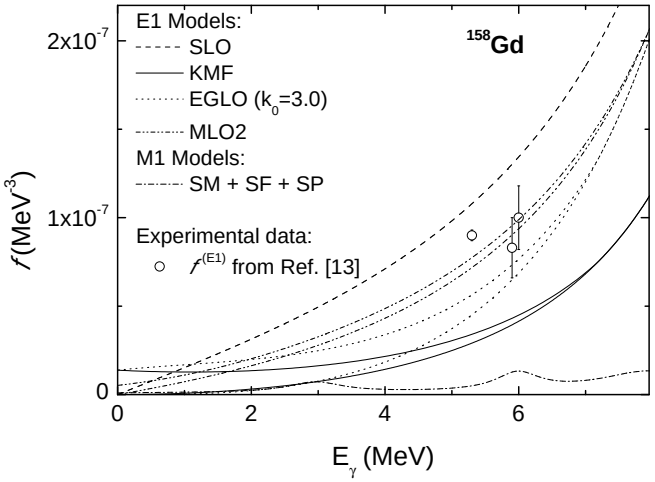

FIG. 2: PSF models used in simulations. There are two curves for the KMF, EGLO, and MLO2 models shown. They indicate how these two models change as a function of temperature - the lower curve corresponds to $T = 0$ while the upper one to $T = \sqrt{(B_n - E_f)/a}$. Experimental data for f_{E1} are for ^{155,157,159}Gd at energies 5.9, 6.0 and 5.3 MeV, respectively [13].

2. *Magnetic-dipole transitions*

Magnetic dipole ($M1$) transitions also play an important role in the decay of highly excited nuclear states. Usually, two models are used for $M1$ transitions. In the spin-flip (SF) resonance model $f_{\rm SF}^{(M1)}(E_\gamma)$ is usually assumed to have a Lorentzian shape with energy about 7 MeV and width of 4 MeV [13], while in the single-particle model $f_{\rm SP}^{(M1)}$ is a constant independent of γ-ray energy. The $M1$ strength corresponding to the spin-flip mode was measured for several rare-earth nuclei (including ^{158}Gd) from inelastic proton scattering [18]. A double-humped structure was observed between 5 and 10 MeV and we adopted this form of SF resonance in our simulations.

Sometimes a sum of the strengths from the two models, $f_{\rm SP}^{(M1)}$ and $f_{\rm SF}^{(M1)}$, is used. In our simulations we usually adjusted the absolute value of the PSFs to obtain the ratio of $f^{(E1)}/f^{(M1)} \approx 7$ at about 7 MeV. This value seems to be reasonably well determined from average resonance capture experiments [19].

3. *Scissors mode*

In 1976, Hilton [20] and later Lo Iudice and Palumbo [21], using the geometrical two rigid rotors model, and Iachello [22], using the proton-neutron interacting boson model, predicted an isovector $M1$ collective vibrational mode in deformed nuclei. This mode, known as the scissors mode (SM), was experimentally observed for ground-state transitions by Bohle *et al.* [23] from high-resolution electron inelastic scattering at low momentum

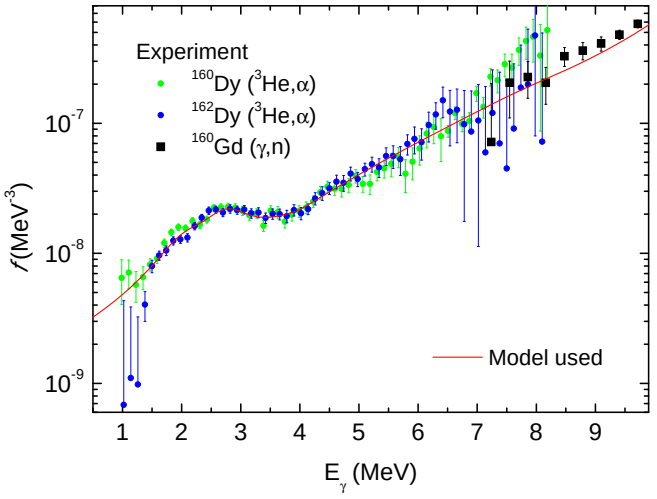

FIG. 3: (Color online) Experimental data on the PSF determined from ^{3}He-induced reactions [30]. The curve shows a model of the PSFs which reproduces these experimental data reasonably well and which was tested in our simulations (see Sec. V).

transfer. The parameters of the mode for transitions to the ground state were intensively investigated using the (γ,γ') reaction in rare-earth nuclei; this revealed substantial fragmentation of the mode. These experiments concluded that the strength of the mode (or more precisely the total $M1$ strength in the energy range $E_\gamma \approx 2.5-4.0$ MeV) for the ground-state transitions in even-even rare-earth nuclei is proportional to the square of the deformation [24]; for well deformed nuclei this strength reaches $B(M1) \approx 3\mu_N^2$. The published experimental value for ^{158}Gd is $B(M1) = 3.71(59)\mu_N^2$ [25] or $3.39(17)\mu_N^2$ [26]. The centroid of the scissors mode strength is located near 3 MeV and is almost constant in rare-earth nuclei; the experimental value for ^{158}Gd is $E_{\rm SM} = 3.10$ MeV [25, 27]. In our simulations the scissors mode was represented by a single or double Lorentzian resonance term.

The analysis of data on two-step γ cascades (TSC) [28, 29] revealed that the scissors mode is not only built on the ground state, but also plays a role in transitions between excited states. In other words, the scissors mode follows, at least approximately, the Brink hypothesis. This finding has been later supported by data from ^{3}He-induced γ emission [30].

Data on the photon strength function inferred from the (^{3}He,$\alpha\gamma$) reaction for neighboring even-even nuclei ^{160}Dy and ^{162}Dy [30] are shown in Fig. 3. They seem to be in very good agreement and one can also expect similar results for ^{158}Gd. The position of the resonance structure at low excitation energies (which is likely the scissors mode) is clearly shifted down to energies lower than 3 MeV in this case.

4. *Electric-quadrupole transitions*

In addition to dipole transitions, electric quadrupole ($E2$) transitions might also play a role in the decay of neutron resonances. We found that $E2$ transitions are not important in the interpretation of our data; we simply assumed the validity of the single-particle model ($f^{(E2)} = $ const.) in our simulations. The strength of $f^{(E2)} = $ const. was taken to reproduce the ratio with respect to dipole strengths at about 7 MeV from average resonance capture data [19].

C. Nuclear Level density

We mainly used the back-shifted Fermi Gas (BSFG) model [14]

$$\rho(E,J,\pi) = f(J)\, f(\pi)\, \frac{e^{2\sqrt{a(E-E_1)}}}{12\cdot 2^{1/2}\,\sigma_c\, a^{1/4}(E-E_1)^{5/4}}, \quad (8)$$

where a and E_1 are adjustable parameters, while

$$f(J) = \exp\left(\frac{-J^2}{2\sigma_c^2}\right) - \exp\left(\frac{-(J+1)^2}{2\sigma_c^2}\right) \quad (9)$$

is the spin probability distribution function. We adopted two different expressions for the spin cut-off parameter σ_c together with the adjustable parameters a and E_1 from the latest works of von Egidy and Bucurescu [14, 31]. Both of these parametrizations led to virtually the same results in our analysis. No parity dependence was assumed in the BSFG model.

In addition to the closed-form BSFG model, we tested the level density calculated within the Hartree-Fock-Bogoljubov (HFB) approach. Here, the level density is available in tabulated form as a function of energy for levels with each spin and parity [17, 32]. The calculated level densities usually suffer from difficulties in reproducing the average neutron resonance spacing. In order to bring the calculations into agreement with experimental data, the HFB level density was renormalized to reproduce the resonance spacing at the neutron separation energy. After such a renormalization there is very good agreement between the HFB level density and the BSFG model at energies above about 2.5 MeV, see Fig. 4.

All known levels below $E_{\rm crit} = 2.1$ MeV are taken into account in the simulations. The level density formula is thus applied only above this energy. It is interesting to note that the adopted level density models are in excellent agreement with level densities obtained from ^{3}He-induced measurements in neighboring even-even Dy isotopes [33], see Fig. 4.

IV. RESONANCE SPINS

As the resonance spin is expected to have an impact on the γ-ray multiplicity distribution, the γ-ray multi-

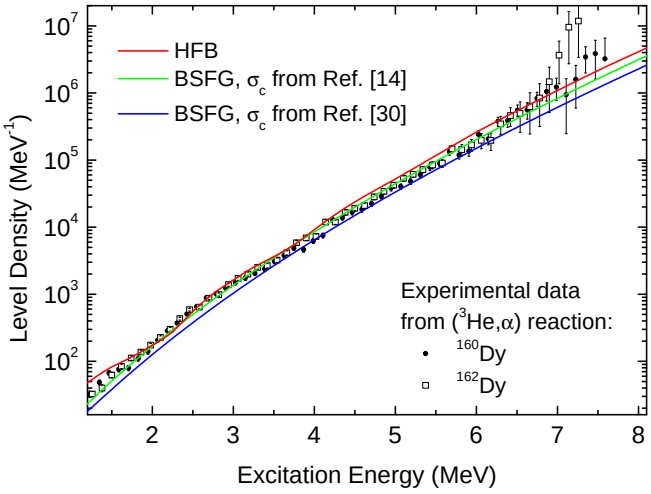

FIG. 4: (Color online) Level density models used in simulations. The different absolute values predicted by the various level density models originate from the different spin distributions for the different models. The resonance spacing of s-wave resonances is the same in all cases. Models of level density are compared with experimental data for even-even Dy isotopes [33].

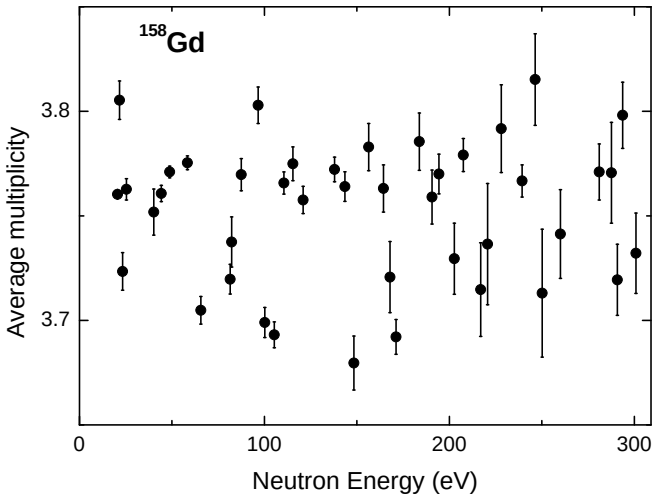

FIG. 5: Average multiplicities of resonances.

plicity of the cascade decay of neutron resonances has been used in a variety of ways to determine the resonance spin. If the distributions from different resonance spins are very different, then the average multiplicity – the simplest quantity characterizing the multiplicity distribution – is sufficient to determine the spin. This was, for instance, true for the s-wave resonances on ^{95}Mo measured with DANCE [34]. On the other hand, for some nuclei the distributions from different spins are indistinguishable. In DANCE measurements this was the case for ^{151,153}Eu [35]. The main quantity that influences the difference among the multiplicity distributions from resonances of different spins is the spin difference between the resonance and the ground state of the nucleus – the higher the difference the larger the effect. In practice the Porter-Thomas fluctuations of the primary transitions from different resonances affect the multiplicity distribution from individual resonances and thus also affect the spin determination.

The average multiplicity $\langle M \rangle$ was calculated as

$$\langle M \rangle = \frac{\sum_{M=3}^{7} M C_M}{\sum_{M=3}^{7} C_M}, \qquad (10)$$

where C_M is the number of counts corresponding to multiplicity M after subtracting the background contribution.

The background contribution for $M \geq 3$, originating from γ rays following the capture of scattered neutrons in Ba nuclei, is small. For the $M = 1$ and 2 spectra the background is much more important for weak resonances, where the background subtraction leads to large uncertainties. We thus decided to omit these multiplicities when determining the average multiplicity. Since the counting rate for $M > 7$ was very low, the highest multiplicity considered in any analysis was $M = 7$. Although data were processed up to $E_n = 700$ eV, detailed analysis could only be performed to 300 eV.

The spin and parity of the ground state of ^{157}Gd is $3/2^-$, and the s-wave resonances have $J^\pi = 1^-$ or 2^-.

Simulations with realistic models of the PSFs and the level density (see discussion below) indicate that the difference in the average multiplicity for resonances with the same spin due to Porter-Thomas fluctuations is very small (rms less than 0.01) compared to the expected difference between the two possible spins of about 0.07. This is in agreement with the experimental data. As Fig. 5 illustrates, the average multiplicities tend to separate into two groups, but the uncertainties in the average multiplicities are significant and become more important with increasing neutron energy, especially for weaker resonances. The summation over the whole resonance region also makes it difficult to say anything about resonance doublets. Therefore we apply analysis methods that rely on more detailed properties of the multiplicity distributions.

A method that takes into account the distribution and not just the average multiplicity was developed by Koehler *et al.* [36]. They combined several multiplicity yields and generated the functions $Z^{(J)}$

$$Z^{(1)} = \sum_{M=a}^{b} Y_M^1(E) - N_1 \sum_{M=c}^{d} Y_M^1(E) = 0 \qquad (11)$$

$$Z^{(2)} = \sum_{M=a}^{b} Y_M^2(E) - N_2 \sum_{M=c}^{d} Y_M^2(E) = 0 \qquad (12)$$

where the multiplicities a, b, c, and d follow the conditions $a \leq b < c \leq d$, N_i is a normalization constant and $Y_M^J(\mathrm{E})$ is the yield for a resonance with spin J and multiplicity M. Using isolated resonances for which the spin J is known, the constants N_i are determined such that

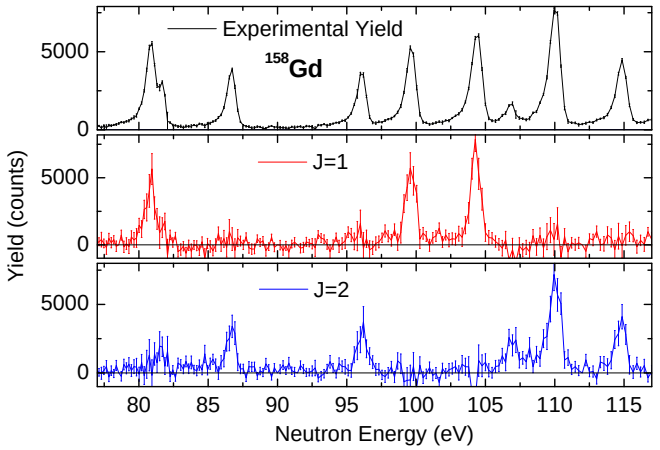

FIG. 6: (Color online) Spin decomposition of the yield for a typical energy region.

the residual yield $Z^{(J)}$ of the resonances with spin J is zero.

Assuming that the multiplicity distribution is the same for resonances with the same spin (approximately true), then applying these equations to an arbitrary neutron energy will give zero or non-zero residuals, depending on the spin composition for the given neutron energy.

Koehler *et al.* took $a = 2, b = 4, c = 5, d = 7$ in ^{147}Sm, but we found that this method also works in ^{157}Gd for $a = b$ and $c = d$, i.e., if only the ratio of two multiplicities is checked. This method would work perfectly if there were no Porter-Thomas fluctuations and experimental errors. DICEBOX simulations with realistic models of the PSFs and the level density show that the Porter-Thomas fluctuations lead to small differences in predicted ratios, which are not large enough to make the method unusable. In practice this approach works well. There are a number of possible combinations of multiplicities, and the results are consistent for the different combinations.

A more formal method was developed by Bečvář *et al.* [37]. In this approach one adopts multiplicity distribution from two resonances of known spin as prototypes and decomposes the actual yield into separate yields for the two spins using the multiplicity distribution as a whole. The results obtained with this method are illustrated in Fig. 6.

The results of applying all above-described methods were very consistent in the region below $E_n = 300$ eV where detailed analysis could be performed. These results were also consistent (with a few exceptions noted below) with the spin values quoted by Mughaghab [38]. There are only three disagreements where we have a definite assignment – resonances at 96.59, 281.02, and 293.70 eV. In each case we assigned $J = 2$ instead of the value of $J = 1$ in Mughabghab. It is interesting that for these three resonances we agree with the assignments of Belyaev *et al.* [39]. Above about 300 eV the combination of poor statistics and worsening energy resolution make

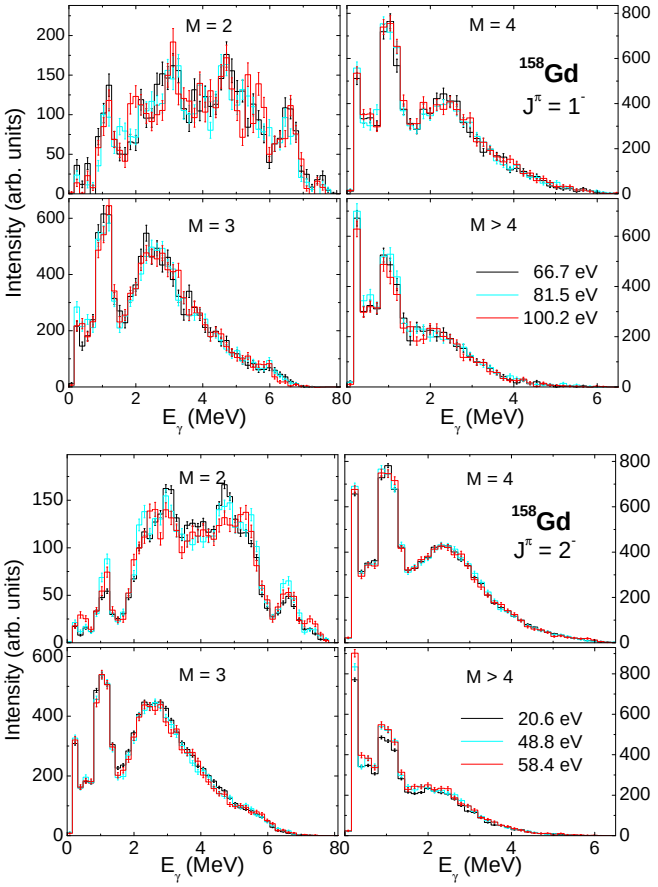

FIG. 7: (Color online) Experimental MSC spectra.

reliable spin assignments impossible.

For ^{157}Gd determining the resonance spins has provided relatively little new information. However, the internal agreement between the various approaches described above, as well as the agreement with the values quoted by Mughabghab and/or Belyaev does establish that the DANCE multiplicity distributions provide a useful tool to determine resonance spins.

V. PROPERTIES OF γ DECAY

A. MSC spectra

In order to obtain information on the properties of the γ decay of ^{158}Gd we compared experimental multistep cascade spectra with predictions based on model simulations described in Sec. III. The MSC spectra were constructed from capture on well-resolved strong resonances. Only γ cascades that deposit virtually all of their energy in the DANCE detector, specifically $7.0 - 8.1$ MeV, were taken into account and sorted according to detected cluster multiplicity. Multiplicities $M = 2 - 7$ were used in the following analysis. In order to minimize statistical uncertainties as well as uncertainties from simulations,

the spectra were binned into coarse bins with a width of 150 keV. As already noted, the background contribution to the MSC spectra is very small for strong resonances.

A large number (several hundreds) of model combinations of PSFs and level densities was tested in simulations and compared with the experimental MSC spectra. It is very difficult to quantify the agreement between simulations and experimental spectra as individual bins in the MSC spectra are mutually correlated in a complicated way, especially due to the decay scheme. As a consequence, the degree of agreement was only checked visually.

For all multiplicities, only one normalization parameter is needed for comparison of experimental and simulated MSC spectra. We normalized spectra to the same number of counts in the $E_{\rm total}$ peak, which includes almost all multiplicities. As already noted, in practice we consider multiplicities $M = 2-7$. The experimental MSC spectra from resonances with the same spin are similar but not identical, due to Porter-Thomas fluctuations of the primary transitions. This is illustrated in Fig. 7.

For the same reason the simulated MSC spectra for different nuclear realizations obtained with the same model of PSFs and level density are not identical. To characterize uncertainties due to Porter-Thomas fluctuations the predicted MSC spectra are plotted as a gray band. Each such band has a width of two sigma (the average $\pm$ one sigma) and was obtained from analysis of 20 independent nuclear realizations. The size of fluctuations among the MSC spectra for different resonances seems to be well reproduced by the simulations. The spectra from different nuclear realizations are almost identical for higher multiplicities ($M \geq 4$), while some differences are predicted for lower multiplicities, especially for $M = 2$.

B. Comparison with experiment

Models that do not include a resonance structure near 3 MeV in a PSF are unable to reproduce the humps at this energy observed in the $M = 2-4$ MSC spectra. A typical example of simulated MSC spectra with no such resonance structure is shown in Fig. 8. This finding is independent of the model adopted for the "non-resonant" part of the PSF.

Simulations also showed that the resonance structure cannot be of $E1$ character. This is because the $M = 2$ spectrum consists mainly of events where neutron resonances with negative parity decay via two γ rays to the ground state which has positive parity. If $E1$ strength dominated the PSF near 3 MeV (which would be the case if the resonance-like structure were in the $E1$ PSF) such decays would not be possible. On the other hand, a resonance structure near 3 MeV in the $M1$ or $E2$ PSF is able to describe the $M = 2$ spectra. We assume in the following that such a resonance structure is in the M1 PSF, i.e., it is the scissors mode.

Assuming that the scissors mode consists of a single-

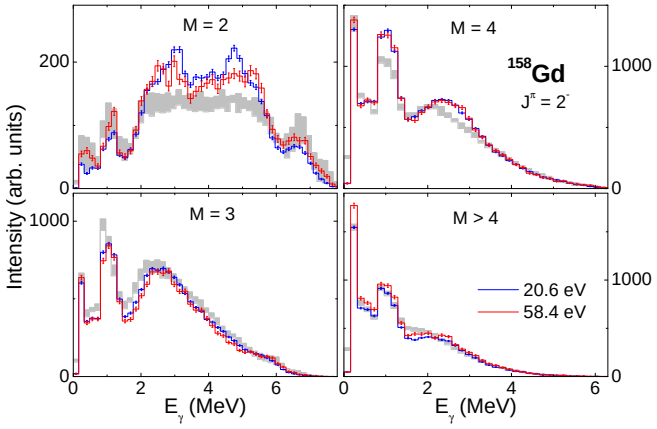

FIG. 8: (Color online) Comparison of experimental MSC spectra with simulations (gray band) in which the scissors mode was completely absent. The combination of $f^{(E1)}_{\rm KMF}$, $f^{(M1)}_{\rm SF} + f^{(M1)}_{\rm SP}$ is used.

Lorentzian term, we found that the MSC spectra are rather sensitive to the energy of the scissors mode, $E_{\rm SM}$. The dependence of the MSC spectra on the resonance damping width, $\Gamma_{\rm SM}$, and on the total strength of the scissors mode – which is given by the product $\sigma_{\rm SM}.\Gamma_{\rm SM}$ – is much weaker.

The position of the mode must be very close to 3 MeV – we estimate that it cannot be lower than about 2.8 MeV or higher than about 3.1 MeV. If the resonance energy is outside this range the shapes of the bumps in the MSC spectra for $M = 2-4$ are not reproduced.

This restriction on the $E_{\rm SM}$ leads, for example, to a disagreement between the present experimental data and simulations with the PSF deduced from (^{3}He,α) in neighboring Dy nuclei, see Fig. 9. The PSF used in these simulations has a resonance structure at about 2.7 MeV, see Fig. 3.

Rather surprisingly, predictions based on very different damping widths yielded similar results. The spectra allow any value between $\Gamma_{\rm SM} = 0.6$ and 1.6 MeV.

We were unable to reach a reasonable agreement between the simulated and experimental spectra for any model combination incorporating the SLO or MLO models for the $E1$ PSF. On the other hand, a reasonably good agreement is achieved with the KMF model, as well as with the EGLO model (with the dimensionless constant k_0 adjusted at values 1.5-3.5), in combination with a "composite" model of the $M1$ PSF: $f^{(M1)} = f^{(M1)}_{\rm SM} + f^{(M1)}_{\rm SF} + f^{(M1)}_{\rm SP}$. The simulated MSC spectra are virtually insensitive to $\sigma_{\rm SM}$ within the range of $0.07-0.25$ mb and to $f^{(M1)}_{\rm SP}$ within the range $(1-2.5)\times10^{-9}$ MeV^{-3}. The most pronounced sensitivity to σ_{SM} is observed in the $M = 3$ spectrum – the larger σ_{SM} the more pronounced the bump near 3 MeV.

Examples of predicted MSC spectra for two of these model combinations, one incorporating the KMF model and the other the EGLO model for the $E1$ PSF, are

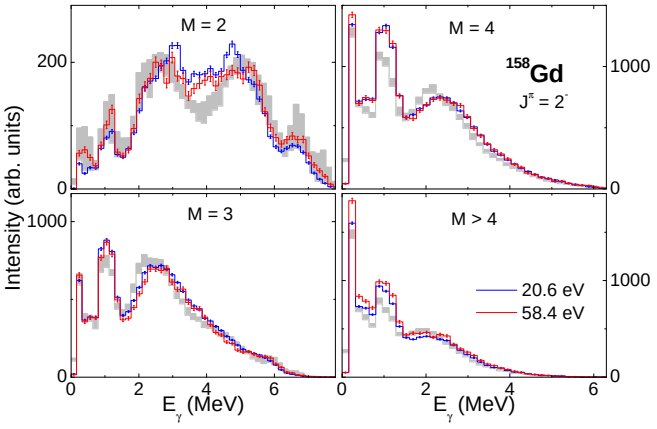

FIG. 9: (Color online) Comparison of experimental MSC spectra with simulations (gray band) for the model determined from ^{3}He-induced reactions. The PSF used is shown in Fig. 3.

shown in Fig. 10, with the set of parameters for the $f^{(M1)}$ PSF specified in the figure caption. The PSFs used in these simulations are shown in Fig. 2. Omitting the $f_{\rm SP}^{(M1)}$ part of $M1$ PSF worsens the agreement in all tested cases. There is only a very slight sensitivity of the shapes of simulated spectra to the parameters of $f_{\rm SF}^{(M1)}$ and to the $E2$ strength. Also, there is virtually no difference among predictions made with BSFG models of level density and the level density based on HFB calculations. The agreement between simulations and experiment is also worse if the scissors mode is not postulated at all levels, i.e., if it violates the Brink hypothesis.

The values inferred for the energy of the scissors mode, $E_{\rm SM}$, and its damping width, $\Gamma_{\rm SM}$, are independent of the absolute size of the non-resonant part of PSF strength underlying the scissors mode. On the other hand, the resonance cross section, $\sigma_{\rm SM}$, is expected to depend on the strength of this non-resonant part of the PSF, since the γ decay is governed only by the ratios of PSFs for different multipolarities and their energy dependence. However, we found that very similar values of $\sigma_{\rm SM}$ are consistent with both the KMF and EGLO models of the $E1$ PSF.

Based on a large number of simulations with different assumptions about the shape and structure of the resonance near 3 MeV, we believe that the description of the scissors mode with a single-resonance term is not unique. Similar agreement to that in Fig. 10 can be obtained with "more complex" models of the resonance, if the total width and strength of the resonance structure are similar to those of the single-Lorentzian term. Specifically, very good agreement was reached for a double-Lorentzian structure of the resonance term with energies at about 2.5 and 3.1 MeV, see Fig. 11. The strict validity of the Brink hypothesis for the $M1$ scissors mode was assumed in all of these cases.

We should stress that within an enormous functional space the trial-and-error method adopted in our analysis does not guarantee that we find the models (or combinations of parameters) that lead to the best possible agreement between simulated and experimental MSC spectra.

None of the tested models was able to correctly describe the strength of the peak at $E_\gamma \sim 1$ MeV in the MSC spectra for $M \geq 3$, while the position and the width were well reproduced in all cases. The peak is a consequence of transitions connecting the lowest negative-parity states, occurring at excitation energies $\sim 1 - 1.3$ MeV, with the ground-state band levels. Reasonable reproduction of the strength (or height) of the peak in the $M = 2$ spectrum indicates that the direct feeding of negative-parity levels near 1 MeV from resonances is simulated correctly.

The underestimation of the predicted strength of the peak in the spectra for higher multiplicities indicates that the population of these lowest negative-parity levels is too low in our simulations. The most likely explanation is that the decay of some of the levels above $E_{\rm crit}$ is not completely controlled by statistical considerations. This is probably not that surprising for levels just above 2 MeV. However, the overall agreement between the simulated and experimental spectra indicates that this possible "non-statistical" contribution influences only a small part of the decays and does not change our conclusions about the scissors mode.

With the exception of the SLO model and the model based on data from ^{3}He induced reactions, we did not test models where the $E1$ PSF does not depend on temperature (or in other words models that fully obey the Brink hypothesis). As a consequence, we are unable to decide whether we need a temperature-dependent $E1$ PSF in order to reproduce the MSC spectra. We can only conclude that the MSC spectra are consistent with predictions of "temperature-dependent" KMF or EGLO models.

VI. COMPARISON WITH OTHER DATA

There are several other relevant measurements that provide information on the PSFs below the neutron separation energy both for this nuclide and for other nuclei in the $A \sim 160$ mass region.

Data on ground-state transitions from (γ,γ') measurements [25, 26], that are available for many even-even nuclei, and data from ^{3}He-induced reactions [30] were mentioned previously.

In addition, there also exist data from the (n,γ) reaction. Specifically, (i) values of the PSFs were obtained from the intensities of primary transitions from resonance neutron capture in neighboring odd nuclei [13], (ii) two-step γ cascades following thermal neutron capture in ^{162}Dy were measured [29], and (iii) information on the total radiation widths of neutron resonances is available for all stable isotopes [38].

Simulations with a PSF model that described well data from the (^{3}He,α) reaction on neighboring even-even nuclei were compared with our experimental data in Fig.

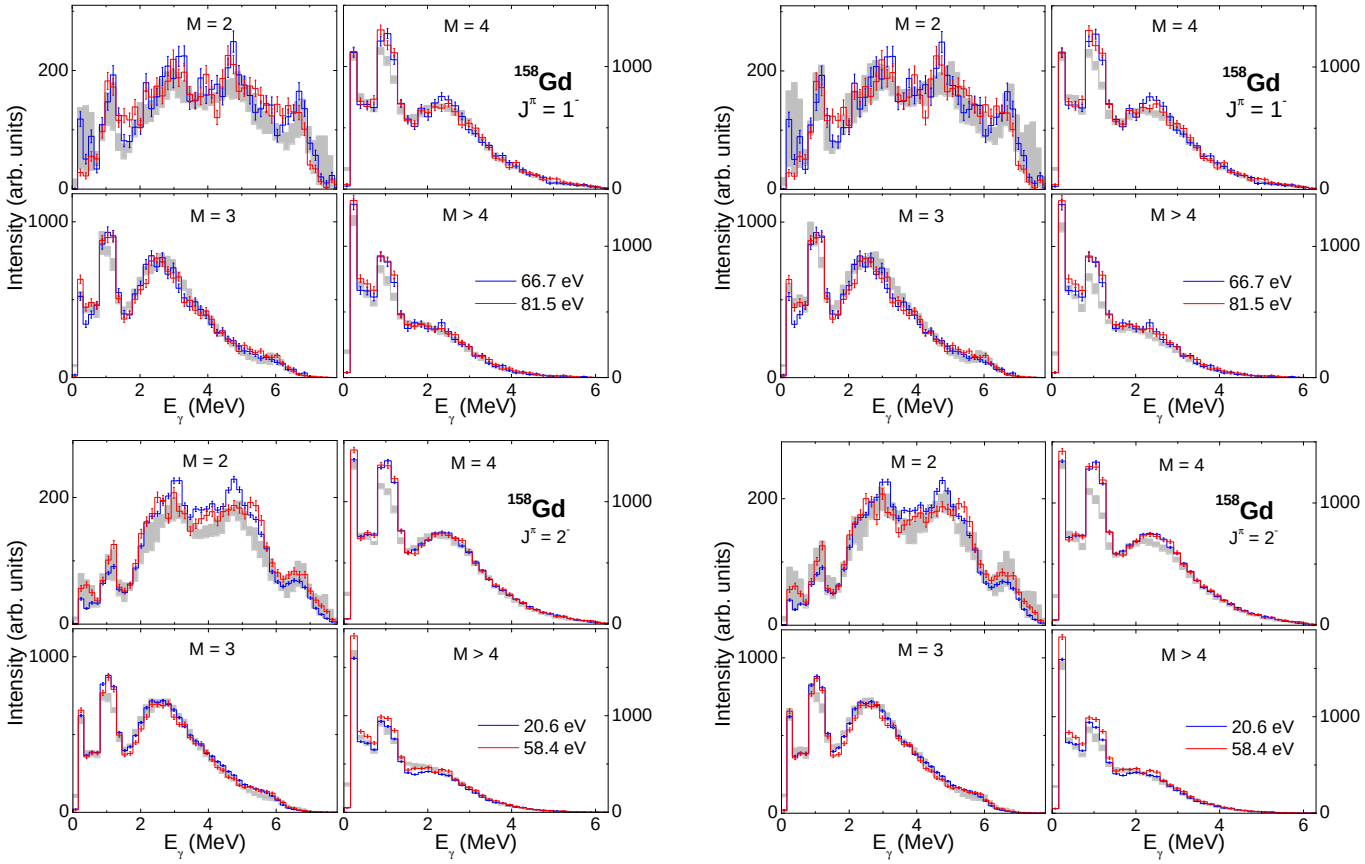

FIG. 10: (Color online) Comparison of experimental MSC spectra with simulations (gray band) made with the model combination of $f^{(E1)}_{\rm KMF}$, $f^{(M1)}_{\rm SM}+f^{(M1)}_{\rm SP}+f^{(M1)}_{\rm SF}$ (left) and the combination $f^{(E1)}_{\rm EGLO}(k_0=3.0)$, $f^{(M1)}_{\rm SM}+f^{(M1)}_{\rm SP}+f^{(M1)}_{\rm SF}$ (right). Parameters of the scissors mode were $E_{\rm SM}=3.0$ MeV, $\Gamma_{\rm SM}=1.0$ MeV, and $\sigma_{\rm SM}=0.2$ mb, and $f^{(M1)}_{\rm SP}=1\times10^{-9}$ MeV^{-3}.

TABLE II: Total reduced strength of the scissors mode corresponding to various parametrizations. The last two columns give the total strength of the scissors mode, $B_{\rm tot}$, and the strength within the range 2.7-3.7 MeV, $B_{\rm NRF}$, which is reported in the nuclear resonance fluorescence (γ,γ') experiments. The strength scales linearly with $\sigma_{\rm SM}$. Published experimental values for ^{158}Gd are $B(M1)=3.71(59)\mu_N^2$ [25] or $3.39(17)\mu_N^2$ [26].

$E_{\rm SM}$ (MeV)	$\Gamma_{\rm SM}$ (MeV)	$\sigma_{\rm SM}$ (mb)	$B_{\rm tot}(M1)$ μ_N^2	$B_{\rm NRF}(M1)$ μ_N^2
3.0	0.6	0.2	1.33	0.88
3.0	1.0	0.2	2.13	1.11
3.0	1.6	0.2	3.23	1.26
2.5	0.4	0.1		
3.1	0.8	0.2	2.23[a]	1.14[a]

[a] Double-humped scissors mode.

9. From the comparison it is evident that the position of the resonance-like structure observed in this reaction at about 2.7 MeV is too low to agree with our MSC spectra. The difference between the PSFs deduced from (n,γ) and (^{3}He,α) reactions remains unexplained.

As already mentioned in Sec III.B.3., the data from (γ,γ') yield the total reduced $M1$ strength for transitions to the ground state of $B(M1)\approx3.5\mu_N^2$ for E_γ between 2.7 and 3.7 MeV in ^{158}Gd. As it is evident from Tab. II, where the strength of the mode used in our simulations is listed, our data require significantly smaller $B(M1)$. In fact, we should not compare only the strength of the scissors mode, but rather the sum of all $M1$ contributions, $f^{(M1)}=f^{(M1)}_{\rm SM}+f^{(M1)}_{\rm SP}+f^{(M1)}_{\rm SF}$, with experimental data. The $f^{(M1)}_{\rm SF}$ contribution to the given energy interval is very weak, about $0.15\mu_N^2$. The contribution of $f^{(M1)}_{\rm SP}$ is slightly higher – the $f^{(M1)}_{\rm SP}=1\times10^{-9}$ MeV corresponds to $B(M1)=0.26\mu_N^2$ – and $B(M1)$ scales linearly with the value of $f^{(M1)}_{\rm SP}$. In any case, the $B(M1)$ needed for reproduction of our data is at most about $2\mu_N^2$. The observed difference in the strengths suggests that the parameters of the scissors mode for ground-state transitions differ from the corresponding parameters for excited levels. Such a situation would not be at variance with our data as simulations with the SM that gives $B(M1)\sim3\mu_N^2$ for the ground state transitions but $B(M1)\sim1.1\mu_N^2$ for transitions between all excited states showed negligible difference with respect to simulations with the SM giving $B(M1)\sim1.1\mu_N^2$ independently of

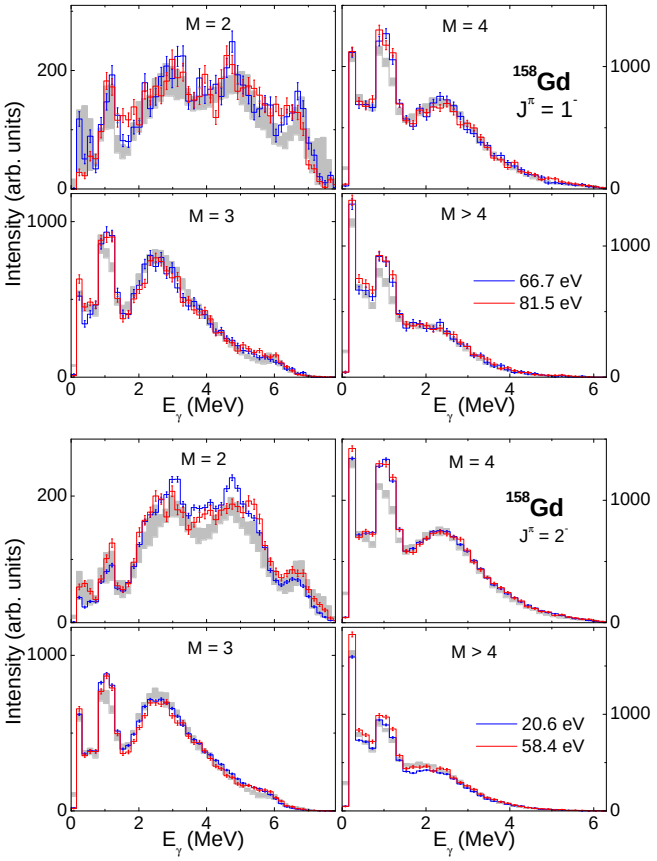

FIG. 11: (Color online) Comparison of experimental MSC spectra with simulations (gray band) for a model $f^{(E1)}_{\rm KMF}$, $f^{(M1)}_{\rm SM} + f^{(M1)}_{\rm SP} + f^{(M1)}_{\rm SF}$. The "double-humped" scissors mode was used. The parameters of the scissors mode were $E_{\rm SM}$ = 2.5 and 3.1 MeV, $\Gamma_{\rm SM}$ = 0.5 and 0.8 MeV, and $\sigma_{\rm SM}$ = 0.1 and 0.2 mb, respectively.

the final level. In this connection it is interesting to note that the strength determined for the scissors mode resonance in ^{158}Gd is significantly smaller than the strength obtained from the (n,γ) reaction in ^{163}Dy [28, 29]. This implies that the strength of the mode may also significantly differ in odd and even nuclei.

Intensities of primary transitions from (n,γ) reactions on neighbor odd nuclei, see Fig. 2, indicate that an acceptable description of f_{E1} at $E_\gamma \approx 6$ MeV is given by EGLO model. The KMF model significantly underpredicts the experimental data (while the SLO model overpredicts them). Unfortunately, there are no available data on even-even nuclei. Since there is no odd-even A effect observed in the f_{E1} PSF above neutron separation energy, it seems to be reasonable to expect similar values in odd and even-even nuclei at about 6 MeV.

The average total radiation widths, Γ_γ, predicted with the KMF and EGLO($k_0 = 3.0$) models of the $E1$ PSF are about 70-80 meV and 95-105 meV (depending on the exact parameters used for the $M1$ PSF), respectively. From simulations we expect that fluctuation of Γ_γ from different resonances is small – at a maximum about 5 meV (independent of the models used).

Comparison with the experimental value, $\Gamma^{(\rm exp)}_\gamma$ = 97(22) meV, indicates that the PSF models reproducing the MSC spectra give reasonable agreement with the experimental Γ_γ. It should be stressed that the total radiation width is the only one of the simulated quantities that depends on the absolute value of the PSFs. All other observables depend only on the ratios of PSFs for different types of transitions and their energy dependence, but not on the absolute values of the PSFs. Unfortunately, Γ_γ also depends strongly on the energy and spin dependence of the level density which prevents the use of the radiation width for absolute normalization of the PSFs. Assuming that the level density used in the simulations is correct, the KMF model for $E1$ will reproduce the total radiation width if it is multiplied by a factor of about 1.2-1.3. Under these assumptions the M1 strength should be multiplied by the same factor.

VII. SUMMARY

Measurement of γ-ray spectra from resonances in the ^{157}Gd(n,γ) reaction was performed with an isotopically enriched target at the DANCE detector array at LANSCE. The total angular momentum of the s-wave resonances was determined for neutron energies up to E_n = 300 eV with the aid of the multiplicity distributions of the γ-ray decay from the resonances. There was excellent overall agreement with the previous spin assignments.

The MSC γ-ray spectra for different multiplicities from resonances with different spins were used to test the validity of various PSF models. For the $E1$ PSF we found that, at least at low γ-ray energies, a reasonable description was obtained with the model of Kadmenskij, Markushev and Furman [12] or with models that are derived from the KMF approach. On the other hand, data on the PSF obtained from intensities of primary transitions from (n,γ) reactions indicate that much higher strength than that predicted by the KMF model is required for energies only slightly below the neutron binding energy [13, 40, 41]. This indicates that the EGLO model (or model similar to it) appears to be a reasonable model for the $E1$ PSF in deformed rare-earth nuclei.

Our analysis indicates that a resonance-like structure at $E_\gamma \approx 3$ MeV in ^{158}Gd is required in a PSF. The structure is not only a property of the ground-state transitions but must also be present in the decay between excited levels. We identify this structure with the scissors mode as it cannot be in the $E1$ PSF. Our data are unable to distinguish whether the structure consists of a simple single-resonance term or if it is more complicated (two resonances). However, we can conclude that it is relatively wide – we estimate its width to be 0.6-1.6 MeV. In addition to the scissors mode additional "smooth" $M1$ strength is needed to reproduce our data.

The strength of the mode from our data is signifi-

cantly smaller than that of the ground-state transitions from (γ,γ') in even-even rare-earth nuclei, which suggest that the properties of the mode might be different for the ground-state transitions and for transitions between excited levels. However, one cannot exclude a systematic decrease of the scissors mode strength with the excitation energy of the levels on which this mode is based. The strength determined is also much smaller than that observed in the (n,γ) reaction in ^{163}Dy [28, 29]. This points out that the strength of the scissors mode may differ in odd and even nuclei. It is also difficult to understand the difference between the properties of the mode determined from the (^{3}He,α) Oslo data and from the (n,γ) reaction. All of these problems indicate that the properties of the scissors mode and of the PSF at energies below neutron separation energies in general are not fully understood. Further study is needed.

Acknowledgments

This work was supported in part by the U. S. Department of Energy Grants No. DE-FG52-09NA29460 and No. DE-FG02-97-ER41042. This work benefited from the use of the LANSCE accelerator and was performed under the auspices of the U. S. Department of Energy at Los Alamos National Laboratory by the Los Alamos National Security, LLC under Contract No. DE-AC52-06NA25396 and at the Lawrence Livermore National Laboratory by the Lawrence Livermore National Security, LLC under Contract No. DE-AC52-07NA27344. It was also supported by the research plans MSM 0021620859, and INGO LA08015 of the Ministry of Education of the Czech Republic, and grant SVV-2011-263309 of the Charles University in Prague.

[1] P. W. Lisowski *et al.*, Nucl. Sci. Eng. **106**, 208 (1990).
[2] M. Heil, R. Reifarth, M. M. Fowler, R. C. Haight, F. Käppeler, R. S. Rundberg, E. H. Seabury, J. L. Ullmann, and K. Wisshak, Nucl. Instrum. Methods Phys. Res. A **459**, 229 (2001).
[3] R. Reifarth *et al.*, Nucl. Instrum. Methods Phys. Res. A **531**, 530 (2004).
[4] J. M. Wouters *et al.*, IEEE Transactions on Nuclear Science **53**, 880 (2006).
[5] S. Ritt and P.-A. Amaudruz, MIDAS − Maximum Integrated Data Acquisition System, http://midas.psi.ch.
[6] F. Bečvář, Nucl. Instrum. Methods Phys. Res. A **417**, 434 (1998).
[7] M. Jandel *et al.*, Nucl. Instrum. Methods Phys. Res. B **261**, 1117 (2007).
[8] R. G. Helmer, Nuclear Data Sheets **101**, 325 (2004).
[9] C. E. Porter and R. G. Thomas, Phys. Rev. **104**, 483 (1956).
[10] S. S. Dietrich and B. L. Berman, At. Data and Nucl. Data Tables **38** (1988) 199,
[11] D. M. Brink, Ph.D. thesis, Oxford University, 1955.
[12] S. G. Kadmenskij, V. P. Markushev, and V. I. Furman, Sov. J. Nucl. Phys. **37**, 165 (1983).
[13] J. Kopecky, in *Handbook for Calculations of Nuclear Reaction Data*, Report No. IAEA-TECDOC-1034 (IAEA, Vienna, 1998), p. 97.
[14] T. von Egidy and D. Bucurescu, Phys. Rev. C **72** 044311 (2005).
[15] R. E. Chrien, in *Proc. of the Vth International School on Neutron Physics*, Alushta, Dubna 1987, ed. by B.B. Kolesova and V.R. Sarantseva (Dubna Report No. D3, 4, 17-86-747, 1987).
[16] J. Kopecky, M. Uhl and R. E. Chrien, Phys. Rev. **C 47**, 312 (1993).
[17] R. Capote *et al.*, Nucl. Data Sheets **110** 3107 (2009).
[18] D. Frekers *et al.*, Phys. Lett. **B244**, 178(1990).
[19] L. M. Bollinger and G. E. Thomas, Phys. Rev. **C 2**, 1951 (1970).
[20] R. R. Hilton, in *Proceedings of the International Conference on Nuclear Structure*, Dubna, 1976 (unpublished).
[21] N. Lo Iudice and F. Palumbo, Phys. Rev. Lett. **41**, 1532 (1978)
[22] F. Iachello, Nucl. Phys. A358, 89c (1981).
[23] D. Bohle *et al.*, Phys. Lett. **B137** (1984) 27.
[24] W. Ziegler, C. Rangacharyulu, A. Richter, and C. Spieler, Phys. Rev. Lett. 65, 2515 (1990).
[25] H. H. Pitz, U. E. P. Berg, R. D. Heil, U. Kneissl, R. Stock, C. Wesselborg, and P. von Brentano, Nucl. Phys. A492, 411 (1989).
[26] U. Kneissl, H. H. Pitz and A. Zilges, Prog. Part. Nucl. Phys. **37** (1996) 349.
[27] N. Pietralla *et al.*, Phys. Rev. C **58**, 184 (1998).
[28] F. Bečvář, P. Cejnar, J. Honzátko, K. Konečný, I. Tomandl and R. E. Chrien, Phys. Rev. **C 52** 1278 (1995).
[29] M. Krtička, F. Bečvář, J. Honzátko, I. Tomandl, M. Heil, F. Käppeler, R. Reifarth, F. Voss, and K. Wisshak, Phys. Rev. Lett. 92, 172501 (2004).
[30] A. Schiller, A. Voinov, E. Algin, J. A. Becker, L. A. Bernstein, P. E. Garrett, M. Guttormsen, R. O. Nelson, J. Rekstad, and S. Siem, Phys. Lett. **B633**, 225 (2006).
[31] T. von Egidy and D. Bucurescu, Phys. Rev. C **80** 054310 (2009).
[32] S. Goriely, Nucl. Phys. **A605** (1996) 28.
[33] M. Guttormsen *et al.*, Phys. Rev. C **68**, 064306 (2003).
[34] S. A. Sheets *et al.*, Phys. Rev. C **76**, 064317 (2007).
[35] U. Agvaanluvsan *et al.*, Lawrence Livermore National Laboratory technical report UCRL-TR-234006.
[36] P. E. Koehler, J. L. Ullmann, T. A. Bredeweg, J. M. O'Donnell, R. Reifarth, R. S. Rundberg, D. J. Vieira, and J. M. Wouters, Phys. Rev. C **76**, 025804 (2007).
[37] F. Bečvář, P. E. Koehler, M. Krtička, G. E. Mitchell, and J. L. Ullmann, submitted to Nucl. Instrum. Methods Phys. Res. A.
[38] S. F. Mughabghab, *Atlas of Neutron Resonances*, (Elsevier, Amsterdam), 2006.
[39] F. N. Belyaev, V. P. Bolotskii, B. V. Efimov, and G. V. Muradyan, Sov. J. Nucl. Phys. **52**, 401 (1990).
[40] S. Raman, in *Neutron Capture Gamma-Ray Spectroscopy and Related Topics 1981*, edited by T. von Egidy, F. Gönenwein, and G. Maier, Institute of Physics Conference Series **62**, 357 (1982).
[41] S. Kahane, S. Raman, G. G. Slaughter, C. Coceva, and

M. Stefanon, Phys. Rev. **C 30**, 807 (1984).